ARTICLE

doi:10.1038/nature12305

Structural mechanism of cytosolic DNA sensing by cGAS

Filiz Civril[1]*, Tobias Deimling[1]*, Carina C. de Oliveira Mann[1], Andrea Ablasser[2], Manuela Moldt[1], Gregor Witte[1], Veit Hornung[2] & Karl-Peter Hopfner[1,3]

Cytosolic DNA arising from intracellular bacterial or viral infections is a powerful pathogen-associated molecular pattern (PAMP) that leads to innate immune host defence by the production of type I interferon and inflammatory cytokines. Recognition of cytosolic DNA by the recently discovered cyclic-GMP–AMP (cGAMP) synthase (cGAS) induces the production of cGAMP to activate the stimulator of interferon genes (STING). Here we report the crystal structure of cGAS alone and in complex with DNA, ATP and GTP along with functional studies. Our results explain the broad DNA sensing specificity of cGAS, show how cGAS catalyses dinucleotide formation and indicate activation by a DNA-induced structural switch. cGAS possesses a remarkable structural similarity to the antiviral cytosolic double-stranded RNA sensor 2′–5′oligoadenylate synthase (OAS1), but contains a unique zinc thumb that recognizes B-form double-stranded DNA. Our results mechanistically unify dsRNA and dsDNA innate immune sensing by OAS1 and cGAS nucleotidyl transferases.

Recognition of pathogen- or danger-associated molecular patterns (PAMPs or DAMPs) is crucial for host defence. Innate immunity ensures this recognition through germline-encoded pattern recognition receptors (PRRs) and triggers signalling cascades that result in production of proinflammatory cytokines and type I interferons (IFN-α and IFN-β)[1,2]. Cytosolic DNA arising from intracellular bacteria or viral infections is a powerful PAMP and is also implicated as a DAMP in autoimmune diseases[1,3,4]. Over the past years, a variety of PRRs for cytosolic DNA have been reported: DNA-dependent activator of IFN-regulatory factors (DAI, also known as ZBP1)[5], absent in melanoma 2 (AIM2)[6–8], RNA polymerase III[9,10], leucine-rich repeat (in Flightless I) interacting protein-1 (LRRFIP1)[11], DExD/H box helicases (DDX41, DHX9 and DHX36)[12,13] and IFN-inducible protein IFI16[14]. However, these PRRs are either cell-type- or DNA-sequence-specific, are possible accessory factors (DExD/H proteins), or trigger different pathways such as caspase-1 activation (AIM2) or a β-catenin-dependent signalling pathway (LRRFIP1)[15].

Although the DNA sensor for type I IFN production with broad specificity and cell distribution was not identified until recently, it was known that IRF3 and NFκB activation in response to DNA requires STING (stimulator of interferon genes, encoded by gene *TMEM173* the protein is also known as MITA, MPYS or ERIS), a transmembrane protein that is resident on the endoplasmic reticulum[16–18]. STING colocalizes with DNA *in vivo* but binds DNA only with low affinity *in vitro*[19], suggesting the presence of an additional sensor. Furthermore, STING is a direct PRR for cyclic dinucleotides such as c-di-AMP and c-di-GMP[20], which are signalling molecules in prokaryotes and trigger IFN in response to, for example, intracellular bacteria[21,22].

Recent results identified human c-GMP-AMP (cGAMP) synthase (cGAS, also known as C6ORF150 and male abnormal 21 domain containing 1 (MB21D1)) as a broad-specificity cytosolic DNA sensor[23]. In the presence of DNA cGAS produces cGAMP, which is an endogenous second messenger that activates STING[18], explaining how STING can stimulate IFN in response to both cyclic dinucleotides and DNA. To reveal the mechanism of DNA-stimulated cGAMP synthesis, we determined the crystal structure of porcine cGAS^{Mab21} (residues 135–497, comprising the highly conserved, DNA-stimulated nucleotidyl transferase (NTase) domain) with and without a 14-mer dsDNA ligand and nucleotide substrates, along with functional studies *in vitro* and in living cells.

Crystal structure of cGAS^{Mab21}

cGAS is a 60 kDa protein composed of an unstructured, not well conserved amino-terminal stretch of approximately 130–150 residues followed by a highly conserved Mab21 domain that belongs to the nucleotidyl transferase (NTase) superfamily[24]. To overproduce and crystallize cGAS, it was necessary to genetically remove the unstructured N-terminal tail. The resulting cGAS^{Mab21} used in this study (residues 155/161–522 for human cGAS and residues 135–497 for porcine cGAS) possesses DNA-dependent dinucleotide synthesis activity in the presence of a 50-mer dsDNA that induces IFN in THP1 cells (Fig. 1a and Supplementary Fig. 1a, b). Whereas cGAS also produces cGAMP in the presence of a 40-mer dsDNA, no activity was observed when we omitted either GTP or ATP from the reaction mixture or substituted dsDNA with single-stranded DNA (Supplementary Fig. 1a).

We determined the crystal structure of porcine cGAS^{Mab21} by single-wavelength anomalous dispersion to 2.5 Å resolution using a selenomethionine derivative. After density modification, we could build an initial model, which was completed and refined against the 2.0 Å resolution native data, resulting in good *R*-factors and stereochemistry (Supplementary Fig. 1c and Supplementary Table 1).

The Mab21 domain of cGAS comprises two lobes, separated by a deep cleft (Fig. 1b). Lobe 1 possesses the NTase fold with a two-leaved highly twisted β-sheet (β1–β8) that is flanked on the outside by two long α-helices (αA and αB). At the inner side, lining the cleft, β1 and β6 harbour the signature catalytic site residues (E200, D202, D296) of the NTase superfamily that coordinate the catalytic Mg^{2+} ions and nucleotides. Lobe 2 is a bundle of four α-helices (αE–αH), connected

[1]Department of Biochemistry and Gene Center, Ludwig-Maximilians-University, 81377 Munich, Germany. [2]Institute for Clinical Chemistry & Clinical Pharmacology, Unit for Clinical Biochemistry, University Hospital, University of Bonn, 53127 Bonn, Germany. [3]Center for Integrated Protein Sciences, 81377 Munich, Germany.
*These authors contributed equally to this work.

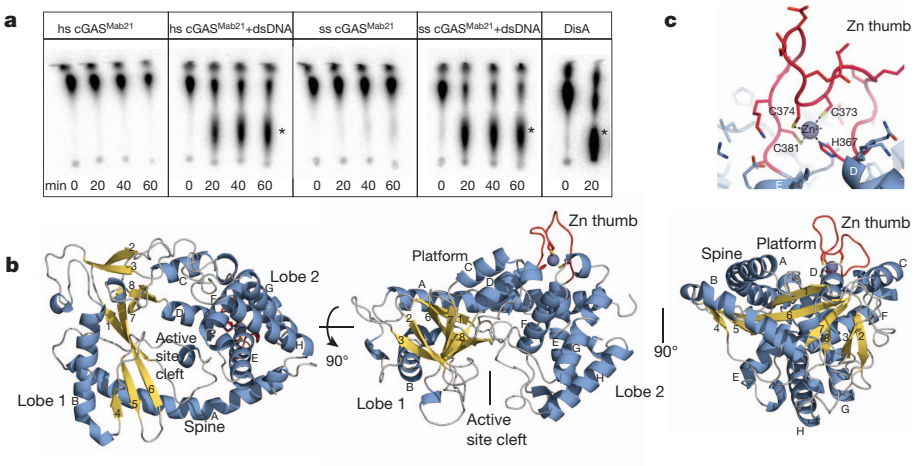

Figure 1 | Crystal Structure of cGAS^{Mab21}. **a**, Activity assays of human and porcine cGAS^{Mab21} alone or in presence of dsDNA. *Bacillus subtilis* DisA, a c-di-AMP synthase is used as positive control. The dinucleotide products are indicated with asterisks. **b**, Side and top views of cGAS^{Mab21}. The model is shown as ribbon representation with annotated domains and secondary structure (blue α-helices, yellow β-strands). **c**, Close-up view of the 'zinc thumb'.

to lobe 1 by a long 'spine' (αA), two linker helices (αC, αD) and by a long active site loop connecting αA and β1.

The molecular surface opposite the active site is a fairly flat, slightly concave 'platform', formed predominantly by αA, αC, αD and the nucleotide-binding loop. An intriguing protrusion (residues 367–382) is situated at one end of the platform. This protrusion contains highly conserved histidine and cysteines (H367, C373, C374 and C381), which together coordinate a Zn^{2+} ion (Fig. 1c). We denote this loop 'Zn thumb'. Its sequence is inserted between lobes 1 and 2 and is a highly conserved and characteristic feature of cGAS orthologues (Supplementary Fig. 1d), indicating an important functional role.

The cGAS–DNA–GTP–ATP complex

To reveal the structure of the activated conformation of cGAS, we co-crystallized cGAS$^{Mab21(td)}$ with a self-complementary 14-mer oligonucleotide, ATP, GTP and $MgCl_2$. To trap an activated conformation of cGAS^{Mab21} with DNA and bound nucleotides we mutated the NTase catalytic residues E200 and D202 to Q and N, respectively, thereby preventing catalysis during crystallization. The resulting transferase-deficient (td) variant is denoted cGAS$^{Mab21(td)}$. The structure of the cGAS$^{Mab21(td)}$–DNA–GTP–ATP complex was determined by molecular replacement using the coordinates for apo cGAS^{Mab21} as search model. $2F_o - F_c$ and $F_o - F_c$ maps revealed interpretable density for 13 out of 14 base pairs of the dsDNA duplex and for both nucleotides bound at the active site (Supplementary Fig. 2). The structure was refined at 3.1 Å resolution, resulting in a model with good *R*-factors and stereochemistry (Supplementary Table 1).

DNA is bound along the platform between the spine on one side and the Zn thumb on the other side (Fig. 2a). cGAS binds DNA predominantly by sequence-independent interactions to both phosphate-sugar backbone strands along the minor groove (Fig. 2b, c). Hereby, cGAS binds seven nucleotides at the core of the platform, which are recognized by at least eleven residues via specific side- and/or main-chain contacts. In addition to the phosphate and sugar contacts, two arginine fingers (R150 and R192) are inserted into the minor groove, additionally stabilizing the interaction in a fairly sequence-independent manner. Besides binding to the array of conserved positively charged residues at the bottom of the platform, DNA is also bound by the spine and the Zn thumb. The continuous helix of the spine in apo-cGAS^{Mab21} is interrupted in the DNA complex and a DNA backbone phosphate is bound at the central kink of the spine helix. On the other side of the platform, the Zn thumb contacts the DNA backbone near the major groove. We do not see close, direct polar contacts between Zn thumb and DNA, but do not want to rule out water-mediated interactions here (Supplementary Fig. 2a).

The Zn thumb does not substantially change conformation or location between apo and DNA-bound cGAS. It seems to be a rather rigid element, in which the zinc ion serves as a structural stabilizer of the protruding loop, similar to Zn^{2+} in regulatory domains of RIG-I-like receptors[25]. The location of the Zn thumb at the backbone near the major groove suggests that it may assist in binding to B-form DNA. In support of this, we do not see a substantial perturbation of the bound DNA from canonical B-form DNA.

Altogether, our structure suggests a specific recognition of B-form dsDNA by cGAS through an extended B-DNA binding platform and

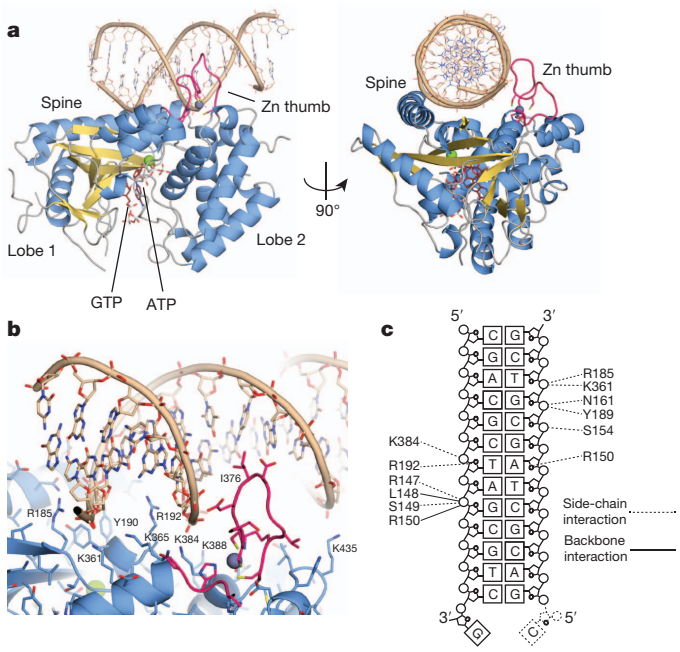

Figure 2 | The cGAS^{Mab21}–DNA–GTP–ATP complex. **a**, Side and top views of cGAS^{Mab21} (colour code of Fig. 1b) in complex with dsDNA (brown), GTP and ATP (ruby stick models). DNA binds along the platform between spine and Zn thumb. **b**, Close-up view of the DNA binding site with selected annotated residues. DNA is bound mainly via the minor groove. A notable exception is the Zn thumb near the major groove. **c**, Schematic representation of DNA–cGAS contacts.

flanking 'Zn thumb' across both lobes of the enzyme. The observed mode of binding is consistent with the key role of cGAS in sensing very different types of DNA in a sequence-independent manner[18,23].

Structure–function analysis

To validate the structural results, we mutated several conserved positively charged residues at the DNA-binding platform of human cGAS, two active site residues, two zinc ligands in the Zn thumb, or the entire Zn thumb and tested for nucleotidyl-transferase activity *in vitro* by thin-layer chromatography (TLC) (Fig. 3a). cGAS produces a product that migrates approximately in the range of c-di-AMP synthesized by DisA[26], consistent with formation of a dinucleotide. The conserved active site residues of NTases (human E225+D227; porcine E200+D202 and human G212+S213) are essential for *in vitro* activity of cGAS^{Mab21}. Moreover, mutation of conserved positively charged residues at the centre and flanking regions of the platform (K173+R176 and K407+K411) either diminish or abolish activity, in accordance with this site being important for DNA sensing. Finally, disruption of the zinc-binding site of the thumb (human C396+C397, Zn thumbless) abolishes DNA-induced NTase activity *in vitro*, highlighting the functional importance of the conserved Zn thumb in DNA binding.

To test the effect of active site, platform and thumb mutations in living cells, we measured the transactivation of an IFN-β promoter reporter by transiently expressing human cGAS variants in HEK293T cells that stably expressed murine STING (Fig. 3b). Induction of IFN-β by cGAS^{Mab21} (human cGAS$^{155–552}$) in these cells is only moderately reduced compared to wild-type cGAS, showing that the Mab21 domain structurally addressed in this study is the catalytic active functional core of the sensor. The activity of full-length cGAS was abolished when residues of the NTase active site were mutated (E225Q/A+D227N/A or G212A+S213A). Mutating charged platform residues (K173A+R176A; K407A+K411A) substantially reduced the activity of cGAS in living cells. Likewise, disrupting the zinc-binding site of the thumb (C396A+C397A, Zn thumbless) severely compromised cGAS activity. These data validate the *in vitro* biochemical data and emphasize the importance of the structure-derived motifs and elements in living cells.

To see whether Zn thumb and conserved platform surface residues are important for dsDNA binding and activity, we performed electrophoretic mobility shift assays (Fig. 3c). Both porcine and human wild-type cGAS^{Mab21} bind efficiently to dsDNA and, surprisingly, also to dsRNA (Supplementary Fig. 3a, c). The mutations in platform and thumb either did not affect DNA/RNA binding under these conditions, or reduced but did not abolish it (Supplementary Fig. 3b). However, both mutants fail to show DNA-stimulated activity under conditions where they still bind DNA, and dsRNA fails to stimulate activity under conditions where it binds robustly to the protein (Supplementary Fig. 3c, d). Thus, although these analyses validate the functional relevance of the DNA binding platform and Zn thumb on activating cGAS, they suggest that DNA or RNA interactions per se are not sufficient to activate the enzyme, indicating for instance the necessity for a precise DNA-induced structural switch.

NTase and DNA induced structural switch

To reveal the mechanism of activation of cGAS by DNA, we first analysed the NTase mechanism. We see clear electron density for two nucleotide triphosphate moieties (Supplementary Fig. 2b). The two bases partially stack in an approximately 90° rotated orientation and inserted into a hydrophobic/aromatic pocket, sandwiched between

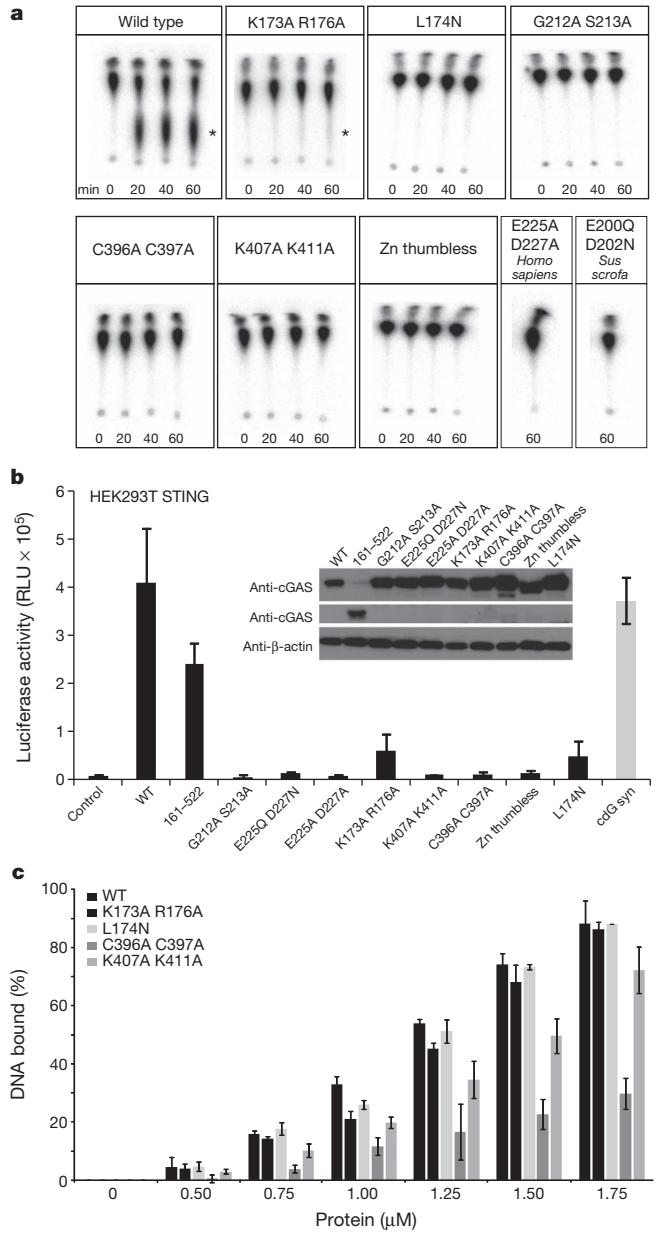

Figure 3 | Platform and Zn thumb are involved in dsDNA-dependent activity. a, NTase assays performed with different cGAS^{Mab21} mutants (2 μM) in presence of 3 μM dsDNA (50-mer). Human wild-type cGAS^{Mab21} (positive control) synthesizes dinucleotide, DNA binding site mutant K173A+R176A show reduced activity. K407A+K411A DNA binding site mutant, C396A+C397A Zn thumb mutant, Zn thumbless, L174N structural switch mutant, active site mutants E200Q+D202N of porcine cGAS^{Mab21} and E225A+D227A and G212A+S213A of human cGAS^{Mab21} are inactive. The asterisk indicates the dinucleotide product. **b**, IFN-β stimulation of cGAS mutants in HEK293T cells stably expressing murine STING. HEK293T cells were transfected with plasmids encoding indicated constructs along with the IFN-β promoter reporter plasmid pIFN-β-GLUC. Luciferase activity is plotted: mean ± s.d. ($n = 3$). Both full-length and the crystallized region (cGAS^{Mab21} human 155–522) induce IFN-β promoter transactivation. Active site mutations (G212A+S213A and E225Q/A+D227N/A) abolish IFN-β stimulation. DNA-binding site mutants (K173A+R176A, K407A+K411A), Zn thumb mutants (C396A+C397A, Zn thumbless) and structural switch mutant (L174N) either reduce or abolish IFN-β stimulation. Empty vector was used as negative control whereas cyclic-di-GMP synthase (cdG syn) expressing vector was used as positive control. Inset: western blot showing wild-type and mutant protein levels with β-actin as loading control. **c**, Electrophoretic mobility shift analysis of 50-mer dsDNA (0.2 μM) bound to cGAS^{Mab21} mutants at indicated concentrations. Plotted bars, mean ± s.d. ($n = 3$). Whereas K407A+K411A DNA binding site mutant and C396A+C397A Zn thumb mutant show slightly reduced but not impaired affinity to dsDNA, no detectable binding change was observed with the other mutants.

I298 (lobe 1) and Y413 (lobe 2). The current resolution of the diffraction data does not allow us to unambiguously determine which base is adenine and which guanine. Binding of R353 at nucleobase 1 (the 'receiving substrate' of NTases) near O6 and N7 would argue for this being guanine. In general, nucleobase 1 (interpreted as guanine here) is in hydrogen bonding distance to S355, S357 and T186, suggesting that this nucleotide is specifically recognized. In contrast, we do not observe direct hydrogen-bonding contacts of the protein to nucleobase 2 (the 'transferred' nucleotide in NTases; interpreted as adenine here). Nevertheless, this recognition might be mediated via water molecules such as in 3′ terminal uridylyl transferases[27].

The structure provides a mechanism for attack of nucleotide 1 on nucleotide 2, consistent with the mechanism of other NTases, for example, CCA adding enzyme[28]. The triphosphate chain of nucleotide 2 is well coordinated via S188 (lobe 1), S412 (lobe 2) and Mg^{2+} bound to E200 (Q in $cGAS^{Mab21(td)}$) and D202 (N in $cGAS^{Mab21(td)}$). As a consequence, the relative orientation of lobes 1 and 2 is important for the phosphate coordination of nucleotide 2. In our conformation, the α-phosphate of nucleotide 2 is well placed and oriented to promote nucleophilic attack of the sugar 2′ OH from nucleotide 1 to form the 2′-5′ linkage (Fig. 4a, see ref. 29). The attacking OH of nucleotide 1 is polarized and activated by D296, consistent with the conserved features of NTases[24]. A second Mg^{2+} could be important for this catalytic step. However, distinct localization will require higher resolution.

cGAS is proposed to form a cyclic-dinucleotide, which would require a second catalysis step and an additional attack of the OH of nucleotide 2 on the phosphate of nucleotide 1. Such an attack will require an almost 180° flip of the sugar moiety of nucleotide 2 to place its α-phosphate appropriately. In principle this is possible: in the course of our studies we determined the crystal structure of $cGAS^{Mab21}$ bound to UTP in the absence of DNA and do observe an appropriate flip of the sugar moiety (Supplementary Fig. 4). In any case, our structure satisfactorily explains the catalysis of formation of a specific (at present linear) dinucleotide by cGAS, but formation of a cyclic dinucleotide needs to be addressed in future studies.

To reveal a potential activation mechanism of cGAS, we superimposed apo-cGAS, $cGAS^{Mab21}$–UTP and $cGAS^{Mab21(td)}$–DNA–GTP–ATP complex (Fig. 4b, c and Supplementary Fig. 5a, b). We used $cGAS^{Mab21}$–UTP because UTP binding orders the β-sheets on lobe 1 and we can also visualize conformational changes specifically induced by dsDNA rather than the nucleotides.

Although UTP binding to cGAS ordered to some extend the nucleotide-binding loop in the active site, it did not substantially change the overall structure and active site geometry of cGAS (Supplementary Fig. 5b). In contrast, DNA phosphate binding to the spine (Fig. 4b) triggers a substantial structural switch in the spine helix (Fig. 4c) that closes lobes 1 and 2 and rearranges the active site loop, allowing magnesium coordinating of E200 to position and activate nucleotide 2.

To test the role of this DNA-induced structural switch we mutated human L174 to N. L174 (porcine L148) is repositioned in response to DNA binding to stabilize the nucleotide-binding loop, but does not directly bind DNA or NTPs (Supplementary Fig. 5c). Although L174N shows fairly normal DNA binding (Fig. 3c and Supplementary Fig. 3b), it lacks DNA-stimulated cGAMP synthetase activity *in vitro* (Fig. 3a) and shows decreased interferon stimulation in cells (Fig. 3b). Thus, the structural and biochemical data suggest that cGAS is activated by a DNA-induced structural switch that rearranges the NTase active site.

Conclusion

Here we provide the structure and mechanism of activation of the cytosolic DNA sensor cyclic-GMP-AMP synthase that readily explain the synthesis of a linear dinucleotide intermediate by cGAS in response to DNA binding. The backbone binding of a canonical B-DNA by cGAS is consistent with a broad specificity innate immune PRR for cytosolic DNA and the structural elements of cGAS such as the positioning of residues involved in minor-groove binding, arginine fingers and the Zn thumb suggest that cGAS specifically responds to B-form DNA. This might explain the function of other innate immune DNA sensors to detect non-canonical DNA structures, such as DAI[5]. A structural switch transmitted by proper B-form DNA binding to the active site could also explain the lack of activation by dsRNA or in mutants that still bind DNA: slightly different conformations of RNA-bound or DNA-bound mutant cGAS would not trigger robust cGAMP synthesis as even small differences in the active site geometry can strongly affect catalytic rates of enzymes.

In future, it will be important to address the specificity for other DNA structures in the activation of cGAS in more detail to see which types of DNA structures can activate cGAS. It will also be important to investigate additional requirements for efficient DNA sensing *in vivo*, because although shorter dsDNA molecules can stimulate $cGAS^{Mab21}$ *in vitro*, DNA larger than 50-mer is required for efficient IFN stimulation *in vivo*[14,19]. One possibility is that fraying of shorter DNA molecules prevents efficient stimulation or that the positively charged N terminus contributes to sensing of longer DNA molecules. In addition, STING might have a direct role in DNA binding in a larger context *in vivo*[19], although we do not see strong DNA binding *in vitro* and IFN stimulation in response to DNA in HEK293T cells in the absence of cGAS (Supplementary Fig. 6).

Interestingly, cGAS has remarkable fold similarity to the antiviral protein oligoadenylate synthase 1 (OAS1)[30,31] (Fig. 5). OAS1 synthesizes 2′-5′ linked oligoadenylate chains in response to binding to

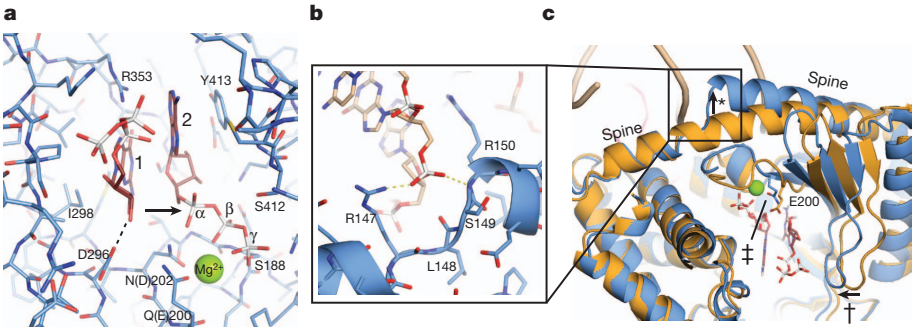

Figure 4 | NTase and DNA-induced structural switch. **a**, Close-up view of the NTase active site. Selected residues that are implicated in binding and catalysis are annotated. Both base moieties partially stack to each other and are further bound by stacking to Y413 and recognition by R353. E200 (mutated to Q in our structure) and D202 (mutated to N in our structure) bind an active site magnesium that coordinates phosphates of nucleotide 2. The attacking OH of nucleotide 1 is activated by D296 for nucleophilic attack on the α-phosphate of nucleotide 2 (arrow). **b**, Close-up view of DNA backbone phosphate binding at the spine. **c**, This DNA phosphate binding triggers a change in the spine helix (*), which allows a closure of the active site cleft (†) and repositioning of the substrate binding loop for Mg^{2+} coordination of E200 (‡).

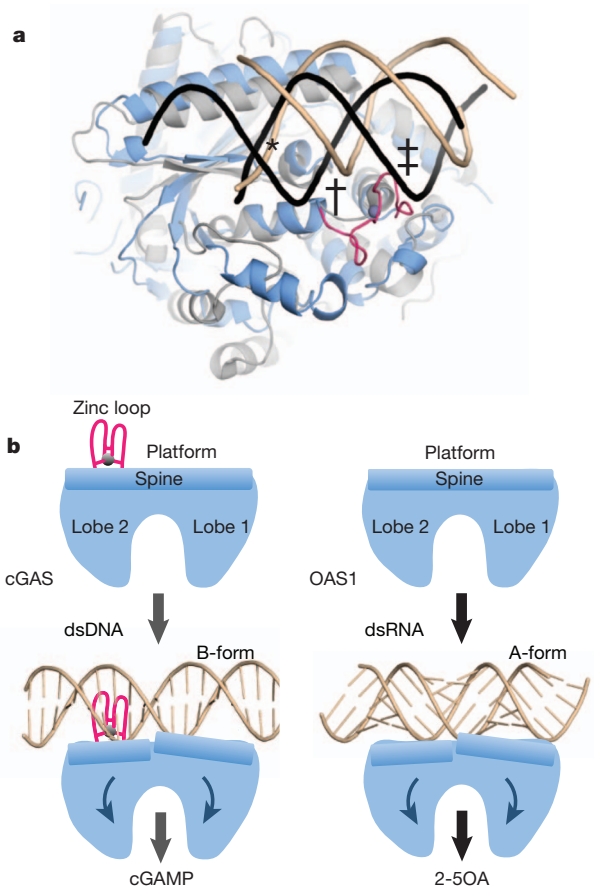

Figure 5 | Model for DNA sensing by cGAS. a, Superposition of cGAS–DNA (blue) with OAS1–RNA (grey) shows key elements for nucleic duplex selectivity. Both enzymes bind one DNA (brown)/RNA (black) backbone at the same protein site (*). The Zn thumb specifically recognizes the position of the second DNA strand in B-form (†).However, it would clash with A-form RNA/DNA (‡). **b**, Unified activation model for cytosolic double-stranded nucleic acid sensing by cGAS and OAS1 NTases by a ligand induced structural switch. 2-5OA, 2′-5′ linked oligoadenylate chains.

cytosolic dsRNA. The structural similarity not only embraces the overall fold, several active site features and arrangement of lobes 1 and 2, but also certain structural elements of the platform, including the long 'spine' helix. Like cGAS, OAS1 binds dsRNA along the 'platform' and triggers a structural change that is transmitted to the active site[31]. However, whereas OAS1 is activated by A-form RNA, cGAS is activated by B-form DNA. The Zn thumb in cGAS, missing in OAS1, probably acts as a molecular 'ruler' to specifically trigger activation in response to B-form but not A-form nucleic acids (Fig. 5). Despite these differences, cGAS shows a structural switch induced by dsDNA that is very similar to that of OAS1 induced by dsRNA[31] (Fig. 5). Thus, our results structurally unify dsDNA and dsRNA sensing by cGAS and OAS1 NTases, respectively, in the innate immune system and suggest that both processes are evolutionarily connected. *Note added in proof*: After submission of the revised version of this manuscript, Gao *et al.*[32] reported related structures of cGAS and its complexes with DNA and nucleotides.

METHODS SUMMARY

Proteins were produced in *Escherichia coli* and purified by affinity, ion exchange and size exclusion chromatography. Apo, UTP- and DNA–ATP–GTP-bound $cGAS^{Mab21}$ and its catalytic inactive form were crystallized by hanging or sitting drop vapour diffusion. The structure of apo $cGAS^{Mab21}$ was determined by single-anomalous dispersion phasing on selenomethionine derivatized protein. The other structures were determined by molecular replacement using apo $cGAS^{Mab21}$ as search model. NTase assays were performed by thin layer chromatography and phosphor imaging. DNA and RNA binding were assessed by electrophoretic mobility shift assays. Analysis of cGAS mutants in living cells were performed in HEK 293T cells stably expressing full-length murine STING and transfected with an IFN-β promoter reporter plasmid.

Full Methods and any associated references are available in the online version of the paper.

Received 21 March; accepted 20 May 2013.
Published online 30 May 2013.

1. Rathinam, V. A. K. & Fitzgerald, K. A. Cytosolic surveillance and antiviral immunity. *Curr. Opin. Virol.* **1,** 455–462 (2011).
2. Takeuchi, O. & Akira, S. Pattern recognition receptors and inflammation. *Cell* **140,** 805–820 (2010).
3. Keating, S. E., Baran, M. & Bowie, A. G. Cytosolic DNA sensors regulating type I interferon induction. *Trends Immunol.* **32,** 574–581 (2011).
4. Krug, A. Nucleic acid recognition receptors in autoimmunity. *Handb. Exp. Pharmacol.* **183,** 129–151 (2008).
5. Takaoka, A. *et al.* DAI (DLM-1/ZBP1) is a cytosolic DNA sensor and an activator of innate immune response. *Nature* **448,** 501–505 (2007).
6. Bürckstümmer, T. *et al.* An orthogonal proteomic-genomic screen identifies AIM2 as a cytoplasmic DNA sensor for the inflammasome. *Nature Immunol.* **10,** 266–272 (2009).
7. Fernandes-Alnemri, T., Yu, J. W., Datta, P., Wu, J. & Alnemri, E. S. AIM2 activates the inflammasome and cell death in response to cytoplasmic DNA. *Nature* **458,** 509–513 (2009).
8. Hornung, V. *et al.* AIM2 recognizes cytosolic dsDNA and forms a caspase-1-activating inflammasome with ASC. *Nature* **458,** 514–518 (2009).
9. Ablasser, A. *et al.* RIG-I-dependent sensing of poly(dA:dT) through the induction of an RNA polymerase III-transcribed RNA intermediate. *Nature Immunol.* **10,** 1065–1072 (2009).
10. Chiu, Y. H., Macmillan, J. B. & Chen, Z. J. RNA polymerase III detects cytosolic DNA and induces type I interferons through the RIG-I pathway. *Cell* **138,** 576–591 (2009).
11. Yang, P. *et al.* The cytosolic nucleic acid sensor LRRFIP1 mediates the production of type I interferon via a β-catenin-dependent pathway. *Nature Immunol.* **11,** 487–494 (2010).
12. Kim, T. *et al.* Aspartate-glutamate-alanine-histidine box motif (DEAH)/RNA helicase A helicases sense microbial DNA in human plasmacytoid dendritic cells. *Proc. Natl Acad. Sci. USA* **107,** 15181–15186 (2010).
13. Zhang, Z. *et al.* The helicase DDX41 senses intracellular DNA mediated by the adaptor STING in dendritic cells. *Nature Immunol.* **12,** 959–965 (2011).
14. Unterholzner, L. *et al.* IFI16 is an innate immune sensor for intracellular DNA. *Nature Immunol.* **11,** 997–1004 (2010).
15. Rathinam, V. A. & Fitzgerald, K. A. Innate immune sensing of DNA viruses. *Virology* **411,** 153–162 (2011).
16. Ishikawa, H., Ma, Z. & Barber, G. N. STING regulates intracellular DNA-mediated, type I interferon-dependent innate immunity. *Nature* **461,** 788–792 (2009).
17. Ishikawa, H. & Barber, G. N. STING is an endoplasmic reticulum adaptor that facilitates innate immune signalling. *Nature* **455,** 674–678 (2008).
18. Wu, J. *et al.* Cyclic GMP-AMP is an endogenous second messenger in innate immune signaling by cytosolic DNA. *Science* **339,** 826–830 (2013).
19. Abe, T. *et al.* STING recognition of cytoplasmic DNA instigates cellular defense. *Mol. Cell* **50,** 5–15 (2013).
20. Burdette, D. L. *et al.* STING is a direct innate immune sensor of cyclic di-GMP. *Nature* **478,** 515–518 (2011).
21. McWhirter, S. M. *et al.* A host type I interferon response is induced by cytosolic sensing of the bacterial second messenger cyclic-di-GMP. *J. Exp. Med.* **206,** 1899–1911 (2009).
22. Woodward, J. J., Iavarone, A. T. & Portnoy, D. A. c-di-AMP secreted by intracellular *Listeria monocytogenes* activates a host type I interferon response. *Science* **328,** 1703–1705 (2010).
23. Sun, L., Wu, J., Du, F., Chen, X. & Chen, Z. J. Cyclic GMP-AMP synthase is a cytosolic DNA sensor that activates the type I interferon pathway. *Science* **339,** 786–791 (2013).
24. Kuchta, K., Knizewski, L., Wyrwicz, L. S., Rychlewski, L. & Ginalski, K. Comprehensive classification of nucleotidyltransferase fold proteins: identification of novel families and their representatives in human. *Nucleic Acids Res.* **37,** 7701–7714 (2009).
25. Cui, S. *et al.* The C-terminal regulatory domain is the RNA 5′-triphosphate sensor of RIG-I. *Mol. Cell* **29,** 169–179 (2008).
26. Witte, G., Hartung, S., Buttner, K. & Hopfner, K. P. Structural biochemistry of a bacterial checkpoint protein reveals diadenylate cyclase activity regulated by DNA recombination intermediates. *Mol. Cell* **30,** 167–178 (2008).
27. Stagno, J., Aphasizheva, I., Rosengarth, A., Luecke, H. & Aphasizhev, R. UTP-bound and apo structures of a minimal RNA uridylyltransferase. *J. Mol. Biol.* **366,** 882–899 (2007).
28. Xiong, Y. & Steitz, T. A. Mechanism of transfer RNA maturation by CCA-adding enzyme without using an oligonucleotide template. *Nature* **430,** 640–645 (2004).
29. Ablasser, A. *et al.* cGAS produces a 2′-5′-linked cyclic dinucleotide second messenger that activates STING *Nature* http://dx.doi.org/10.1038/nature12306 (30 May 2013).

30. Hartmann, R., Justesen, J., Sarkar, S. N., Sen, G. C. & Yee, V. C. Crystal structure of the 2′-specific and double-stranded RNA-activated interferon-induced antiviral protein 2′-5′-oligoadenylate synthetase. *Mol. Cell* **12,** 1173–1185 (2003).
31. Donovan, J., Dufner, M. & Korennykh, A. Structural basis for cytosolic double-stranded RNA surveillance by human oligoadenylate synthetase 1. *Proc. Natl Acad. Sci. USA* **110,** 1652–1657 (2013).
32. Gao, P. *et al.* Cyclic [G(2′,5′)pA(3′,5′)p] is the metazoan second messenger produced by DNA-activated cyclic GMP-AMP synthase. *Cell* **153,** 1094–1107 (2013).

Supplementary Information is available in the online version of the paper.

Acknowledgements We thank A. Butryn for comments on the manuscript. We thank the Max-Planck-Crystallization facility for initial crystal screening and the Swiss Light Source, European Synchrotron Radiation Facility and the German electron synchrotron Petra III for beam time and on-site assistance. This work was funded by the National Institutes of Health (U19AI083025), the European Research Council Advanced Grant 322869, and the Center for Integrated Protein Science Munich (CIPSM) to K.-P.H., by DFG grant 3717/2-1 to G.W., by GRK1721 to K.-P.H. and G.W., by DFG grant SFB670 and ERC grant 243046 to V.H.; C.C.O.M. is supported by GRK1721.

Author Contributions F.C. crystallized and determined the structure of cGAS, performed biochemical assays, interpreted data and wrote the manuscript. T.D. crystallized and refined the DNA complex. C.C.O.M., A.A., T.D. and M.M. performed biochemical assays. G.W. performed biochemical assays, interpreted data and helped with structure determination. V.H. supervised the cell-based experiments and interpreted data. K.-P.H designed the research, helped with structure determination, interpreted data and wrote the manuscript.

Author Information Coordinates and structure factors have been deposited at the Protein Data Bank (4JLX, 4JLZ and 4KB6). Reprints and permissions information is available at www.nature.com/reprints. The authors declare no competing financial interests. Readers are welcome to comment on the online version of the paper. Correspondence and requests for materials should be addressed to K.-P.H. (hopfner@genzentrum.lmu.de).

METHODS

Constructs and cloning. The sequence encoding full-length or truncated *Homo sapiens* and *Sus scrofa* cGAS were amplified from total cDNA (courtesy of S. Bauersachs) and cloned into pIRESneo3 (Clontech) or a modified pET21 (Novagen), respectively. The mutants were generated by site-directed mutagenesis using PfuUltra (Stratagene). Zn thumbless mutant was created by replacing residues 390–405 (*Homo sapiens*) by three Gly-Ser replicates.

Protein production and purification. All proteins were produced in *E. coli* Rosetta (DE3) or B834 (DE3) strains for native or selenomethionine derivative proteins, respectively. Bacteria were grown until a D_{600} of 0.6 to 0.8 was reached and expression was induced at 18 °C for 16 to 18 h with 0.1 mM IPTG. Proteins were purified by Ni-NTA agarose resin and incubated with tobacco etch virus (TEV) protease (ratio 1:50) at 4 °C overnight to remove the 6xHis-MBP-tag. The proteins were further purified by cation exchange chromatography followed by size exclusion chromatography using a Superdex 200 column (GE Healthcare), equilibrated in 20 mM Tris pH 7.5, 150 mM NaCl and 1 mM DTT. Purified proteins were concentrated to 10 mg ml^{-1} for crystallization. Human STING 139–379 was purified as described[33]. All purified proteins were frozen in liquid N_2 and stored at −80 °C.

Crystallization of cGAS^{Mab21}. Purified porcine cGAS (10 mg ml^{-1}) was crystallized by hanging drop vapour diffusion in 20% PEG3350 and 200 mM sodium malonate. The crystals appeared after one day at 20 °C and were flash frozen after addition of glycerol to a final concentration of 15% (v/v). The selenomethionine derivatized protein was crystallized in 100 mM Bis-Tris propane pH 6.3, 18% PEG3350 and 200 mM sodium malonate and cryo protected with 20% ethane-1,2-diol before flash freezing. UTP bound crystals were obtained by adding 20 mM $MgCl_2$ and 1:10 (v/v) of 50 mM of nucleotide in 100 mM Tris pH 7.5 to the protein before crystallization.

For crystallizing the DNA–GTP–ATP–cGAS complex 20 mM $MgCl_2$, 2 mM of both nucleotides and 14 bp dsDNA (5′-CGACGCTAGCGTCG-3′) in a molar ratio of 1:1.2 protein:DNA were added to the inactive porcine cGAS$^{Mab21(td)}$ (E200Q+D202N) (10 mg ml^{-1}). Crystals were obtained by hanging drop vapour diffusion in 50 mM sodium cacodylate pH 7.0, 2.5 mM spermine, 60 mM $MgCl_2$ and 3% (v/v) PEG 400 after one day at 20 °C. The crystals were soaked in reservoir solution containing 25% (v/v) glycerol before flash freezing.

Data collection and refinement. X-ray diffraction data of cGAS and cGAS-UTP were collected at X06SA beamline (Swiss Light Source, Switzerland) and diffraction data of the cGAS$^{Mab21(td)}$–GTP–ATP–DNA complex were collected at PetraIII beamline P14 (EMBL/DESY, Hamburg, Germany) at 100 K. The selenomethionine derivative data were collected at the selenium peak wavelength ($\lambda = 0.97961$ Å). Data processing was carried out with XDS[34]. AutoSHARP was used to locate Se sites (SAD data set) and to produce an initial solvent flattened map[35]. An initial model was built using iterative cycles of Buccaneer[36] and ARP/wARP classic[37]. The model was optimized by alternating manual building with Coot[38] and refinement using Phenix[39] against a 2.0 Å native data set. The structure of UTP-bound cGAS and the DNA–GTP–ATP–cGAS complex structure were determined using molecular replacement with Phaser[40] and optimized by manual building with Coot and refinement with Phenix or Autobuster[41]. Data collection and refinement statistics are listed in Supplementary Table 1.

NTase assays. NTase assays were performed as described in ref. 26. Reaction mixtures with the indicated concentrations of protein and DNA (40-mer: 5′-GGATACGTAACAACGCTTATGCATCGCCGCCGCTACATCC-3′, 50-mer: 5′-GGATACGTAACAACGCTTATGCATCGCCGCCGCTACATCCCTGAGC TGAC-3′) (unless indicated 50-mer dsDNA is used) or RNA (sequence as 50-mer DNA) in 0.1 M NaCl, 40 mM Tris pH 7.5 and 10 mM $MgCl_2$ were started by addition of 100 μM ATP and 100 μM GTP containing 1:600 [α^{32}P]ATP and/or [α^{32}P]GTP (3,000 Ci mmol^{-1}, Hartmann Analytic). Analysis of the reaction products was done using thin layer chromatography (PEI-Cellulose F plates, Merck) with 1 M $(NH_4)_2SO_4$/1.5 M KH_2PO_4 pH 3.8 as running buffer for the TLC plates. Assays were performed at 35 °C. The dried TLC plates were analysed by phosphor imaging (GE Healthcare).

Electrophoretic mobility shift assays. 0.2 μM of dsDNA or dsRNA (same sequences used for NTase assays) was incubated with indicated amount of purified protein for 30 min on ice. As reaction buffer 20 mM Tris pH 8.0 and 200 mM NaCl was used. Samples were separated by 1% agarose gel prepared with Gel-Red (Biotium) as suggested by the manufacturer. The gel images were analysed using ImageJ.

Reporter assays. HEK 293T cells stably expressing full-length murine STING (2×10^4 cells in each well of a 96-well plate) were transiently transfected with 25 ng IFN-β promoter reporter plasmid (pIFN-β-GLUC) in conjunction with 200 ng cGAS expression vectors using GeneJuice (Novagen) as indicated by the manufacturer. A codon-optimized version the diguanylate cyclase domain (83–248) of TM1788 (*Thermotoga maritima* MSB8) harbouring a point mutation (R158A) to enhance c-di-GMP production was cloned into pEFBOS to contain a carboxy-terminal haemagglutinin (HA) tag[42]. This construct (c-di-GMP-synthase) was used to induce c-di-GMP production within 293T cells upon transient overexpression, which served as positive control. 14 h post transfection luciferase activity was assessed.

THP-1 cells were stimulated with 200 ng of either 50-mer dsDNA (as in NTase assays) or tri-phosphate-RNA complexed with Lipofectamine 2000 (Life Technologies) according to the manufacturer's instructions. Supernatants were collected 18 h after stimulation and assayed for IP-10 production via ELISA. 90-mer DNA used is as described in ref. 19. CMA was purchased from Sigma Aldrich.

Immunoblotting. Cells were lysed in 1× Laemmli buffer and denatured at 95 °C for 5 min. Probes were separated by 10% SDS–PAGE and transferred onto nitrocellulose membranes. Blots were incubated with anti-cGAS (Sigma Aldrich), anti-phospho-IRF3 (Cell Signaling Technology) or anti-β-actin-IgG–horseradish peroxidase (HRP). Goat anti-rabbit-IgG–HRP was purchased from Santa Cruz Biotechnology.

33. Cavlar, T., Deimling, T., Ablasser, A., Hopfner, K. P. & Hornung, V. Species-specific detection of the antiviral small-molecule compound CMA by STING. *EMBO J.* **32,** 1440–1450 (2013).
34. Kabsch, W. XDS. *Acta Crystallogr.* **66,** 125–132 (2010).
35. Vonrhein, C., Blanc, E., Roversi, P. & Bricogne, G. Automated structure solution with autoSHARP. *Methods Mol. Biol.* **364,** 215–230 (2007).
36. Cowtan, K. The Buccaneer software for automated model building. 1. Tracing protein chains. *Acta Crystallogr.* **62,** 1002–1011 (2006).
37. Morris, R. J., Perrakis, A. & Lamzin, V. S. ARP/wARP's model-building algorithms. I. The main chain. *Acta Crystallogr.* **58,** 968–975 (2002).
38. Emsley, P. & Cowtan, K. Coot: model-building tools for molecular graphics. *Acta Crystallogr.* **60,** 2126–2132 (2004).
39. Adams, P. D. *et al.* PHENIX: a comprehensive Python-based system for macromolecular structure solution. *Acta Crystallogr.* **66,** 213–221 (2010).
40. McCoy, A. J. *et al.* Phaser crystallographic software. *J. Appl. Crystallogr.* **40,** 658–674 (2007).
41. Blanc, E. *et al.* Refinement of severely incomplete structures with maximum likelihood in BUSTER-TNT. *Acta Crystallogr.* **60,** 2210–2221 (2004).
42. Rao, F. *et al.* Enzymatic synthesis of c-di-GMP using a thermophilic diguanylate cyclase. *Anal. Biochem.* **389,** 138–142 (2009).